

# Structural and Biological Identification of Residues on the Surface of NS3 Helicase Required for Optimal Replication of the Hepatitis C Virus<sup>\*[5]</sup>

Received for publication, November 10, 2005. Published, JBC Papers in Press, November 22, 2005, DOI 10.1074/jbc.M512100200

Samuel G. Mackintosh<sup>†1</sup>, Jeff Zhiqiang Lu<sup>§1,2</sup>, John B. Jordan<sup>§</sup>, Melody K. Harrison<sup>‡</sup>, Bartek Sikora<sup>‡</sup>, Suresh D. Sharma<sup>¶</sup>, Craig E. Cameron<sup>¶</sup>, Kevin D. Raney<sup>‡3</sup>, and Joshua Sakon<sup>§4</sup>

From the <sup>‡</sup>Department of Biochemistry and Molecular Biology, University of Arkansas for Medical Sciences, Little Rock, Arkansas 72205, the <sup>§</sup>Department of Chemistry and Biochemistry, University of Arkansas, Fayetteville, Arkansas 72701, and the <sup>¶</sup>Department of Biochemistry and Molecular Biology, Pennsylvania State University, University Park, Pennsylvania 16802

The hepatitis C virus (HCV) nonstructural protein 3 (NS3) is a multifunctional enzyme with serine protease and DEXH/D-box helicase domains. A crystal structure of the NS3 helicase domain (NS3h) was generated in the presence of a single-stranded oligonucleotide long enough to accommodate binding of two molecules of enzyme. Several amino acid residues at the interface of the two NS3h molecules were identified that appear to mediate a protein-protein interaction between domains 2 and 3 of adjacent molecules. Mutations were introduced into domain 3 to disrupt the putative interface and subsequently examined using an HCV subgenomic replicon, resulting in significant reduction in replication capacity. The mutations in domain 3 were then examined using recombinant NS3h in biochemical assays. The mutant enzyme showed RNA binding and RNA-stimulated ATPase activity that mirrored wild type NS3h. In DNA unwinding assays under single turnover conditions, the mutant NS3h exhibited a similar unwinding rate and only ~2-fold lower processivity than wild type NS3h. Overall biochemical activities of the mutant NS3h were similar to the wild type enzyme, which was not reflective of the large reduction in HCV replicative capacity observed in the biological experiment. Hence, the biological results suggest that the known biochemical properties associated with the helicase activity of NS3h do not reveal all of the likely biological roles of NS3 during HCV replication. Domain 3 of NS3 is implicated in protein-protein interactions that are necessary for HCV replication.

Hepatitis C virus (HCV),<sup>5</sup> a member of the family *Flaviviridae*, is a leading cause of liver cirrhosis and hepatocellular carcinoma and has infected more than 170 million people worldwide (1–3). Standard treat-

ment with interferon- $\alpha$  and ribavirin is frequently ineffective or toxic, and no vaccine for HCV is currently available (4). Identification of a novel viral target for therapeutic intervention could lead to the development of a more effective treatment.

The HCV genome is a 9.6-kb positive, single-stranded RNA that supports translation of a 3000-amino acid polyprotein, which is subsequently cleaved to produce both structural (C, E1, and E2) and nonstructural (NS2, NS3, NS4A, NS4B, NS5A, and NS5B) viral proteins (5). Two viral proteases are encoded by the NS2 and NS3 genes (6, 7). In addition to its protease domain, the NS3 protein also contains a DEXH/D-box helicase domain (8). NS4A encodes a peptide co-factor for NS3 protease (9), and NS5B encodes an RNA-dependent RNA polymerase (10). The functions of NS4B and NS5A have not been as well characterized, but NS5A is involved in viral interferon sensitivity (11) and in adaptation of subgenomic replicons for growth in cultured hepatoma cells (12).

One obstacle to studying viral protein interactions is that HCV cannot be maintained efficiently in cell culture, although recent progress may overcome this difficulty (13). In order to circumvent this problem, selectable replicons carrying the neomycin phosphotransferase gene in addition to essential HCV genes and untranslated flanking regions have been constructed (14). Viral genes are translated independently of the neomycin phosphotransferase gene from an encephalomyocarditis virus internal ribosome entry site. Replication in cell culture has been further enhanced by the introduction of adaptive mutations primarily within the *NS5A* gene (12), although the specific mechanism by which these mutations influence replication is not known. These adaptive replicon mutants provide a means of studying HCV replication in cultured cells.

Many aspects of the HCV replication mechanism remain unknown, but it appears that at least five of the viral nonstructural proteins are required for replication (5). Several nonstructural protein-protein interactions have been identified (15, 16), and co-localization of nonstructural proteins, including NS3 and NS5B, on membrane structures within cells has been observed (17, 18), indicating formation of a multiprotein replication complex containing both polymerase and helicase enzymes. Understanding the mechanism of nucleic acid unwinding by NS3 is therefore a key step in characterizing the viral replication mechanism.

Helicases are molecular motor proteins that utilize energy from ATP hydrolysis to manipulate nucleic acids as well as protein-nucleic acid complexes (19–21). NS3 helicase (NS3h) has been expressed and purified independently of NS3 protease in a recombinant bacterial system and retains its *in vitro* unwinding activity (8). The NS3h structure consists of three distinct domains, with domains 1 and 2 containing all of the

<sup>\*</sup> This work was supported by National Institutes of Health (NIH) COBRE Research Grant P20 RR15569 (to J. S. and K. D. R.), NIH R01 AI060563 (to K. D. R., C. E. C., and J. S.), NIH BRIN Award P20 RR016460, the Arkansas Biosciences Institute, and the United States Department of Agriculture Cooperative State, Research, Education, and Extension Service. The costs of publication of this article were defrayed in part by the payment of page charges. This article must therefore be hereby marked "advertisement" in accordance with 18 U.S.C. Section 1734 solely to indicate this fact.

[5] The on-line version of this article (available at <http://www.jbc.org>) contains supplemental Figs. 1 and 2.

The atomic coordinates and structure factors (code 2F55) have been deposited in the Protein Data Bank, Research Collaboratory for Structural Bioinformatics, Rutgers University, New Brunswick, NJ (<http://www.rcsb.org/>).

<sup>1</sup> These authors contributed equally to this work.

<sup>2</sup> Present address: Dept. of Molecular Microbiology and Immunology, Johns Hopkins Bloomberg School of Public Health, Baltimore, Maryland 21205.

<sup>3</sup> To whom correspondence may be addressed. E-mail: [raneykevind@uams.edu](mailto:raneykevind@uams.edu).

<sup>4</sup> To whom correspondence may be addressed. E-mail: [jsakon@uark.edu](mailto:jsakon@uark.edu).

<sup>5</sup> The abbreviations used are: HCV, hepatitis C virus; NS3h, NS3 helicase domain; MR, molecular replacement; MOPS, 4-morpholinepropanesulfonic acid; r.m.s., root mean square.

conserved motifs common to superfamily II helicase enzymes (22, 23). ATP binds at the interface between domains 1 and 2, and nucleic acid binds within a cleft formed at the interface between domain 3 and domains 1 and 2 (23). Interactions between the protein and nucleic acid are not sequence-specific and primarily involve the phosphate backbone of the nucleic acid.

Despite extensive structural and biochemical characterization, the oligomeric state of the functional species of NS3 has not been determined conclusively. Biochemical studies have resulted in reports of monomeric (24), dimeric (25, 26), and oligomeric (27, 28) forms of the protein. Crystal structures of NS3h (22), NS3h bound to an 8-mer poly(dU) substrate (23), and a full-length NS3/NS4A fusion protein (29) demonstrate that a single protein monomer can form crystals. However, none of these structures includes a substrate molecule of sufficient length to accommodate binding of multiple NS3h monomers. Cross-linking experiments indicate that NS3h can form oligomeric structures in solution (28). DNA unwinding activity of full-length NS3 is optimal at concentrations high enough to allow binding of multiple NS3h monomers to each nucleic acid molecule (30). However, no cooperative effect has been observed in binding studies (31), leaving open the possibility that NS3 is a nonprocessive monomer. A recently reported biochemical model suggests that monomeric NS3h is functional but that multiple NS3h molecules are required for optimal processivity (32).

We have crystallized NS3h bound to a 16-mer poly-dU nucleic acid. The structure shows two NS3h molecules bound to a single DNA molecule and reveals an apparent interface between the two protein molecules. A mutational analysis of the protein interface region was performed in order to determine its importance for helicase activity and viral replication.

## EXPERIMENTAL PROCEDURES

**Purification of NS3h**—BL21(DE3) cells were co-transformed with pET26b expression plasmid containing a wild type or mutant NS3h gene with an NH<sub>2</sub>-terminal ubiquitin tag and pCG1 expressing the ubiquitin protease Ubp1. 3.5 liters of transformed cells were cultured at 37 °C to an A<sub>600</sub> of 1.5 in NZCYM broth containing 30 μg/ml kanamycin and 30 μg/ml chloramphenicol. Overexpression was induced by the addition of 3.5 liters of chilled NZCYM, 0.2% dextrose, and 0.5 mM isopropyl 1-thio-β-D-galactopyranoside. Antibiotic concentrations were kept constant. Cells were cultured at 15 °C for 16–18 h following induction. All subsequent steps were performed at 4 °C. NS3h purification was followed by measuring poly(U)-dependent ATPase activity and by SDS-PAGE. Cells were centrifuged at 6000 rpm for 10 min in a Beckman JLA-10.500 rotor and resuspended in lysis buffer (25 mM Tris/Cl, pH 7.5, 1 mM EDTA, 500 mM NaCl, 5 mM β-mercaptoethanol, 10% glycerol) at 5 ml/g. Cells were lysed by the addition of 4 mM phenylmethylsulfonyl fluoride, 4 μg/ml pepstatin A, and 2.25 mg of lysozyme/g of cells, followed by a freeze/thaw in liquid nitrogen, pressurization at 1500 p.s.i. for 3 min in a nitrogen bomb, and sonication. The lysate was centrifuged at 20,000 rpm for 20 min in a Beckman JA-25.50 rotor. The supernatant was further centrifuged at 45,000 rpm for 2 h in a Beckman 50.2 Ti rotor. The supernatant from the final centrifugation was further purified by anion exchange chromatography. NS3h was eluted in the wash from the anion exchange column with lysis buffer and precipitated by the addition of 55% (NH<sub>4</sub>)<sub>2</sub>SO<sub>4</sub> followed by centrifugation at 20,000 rpm for 60 min in a Beckman JA-25.50 rotor. Pellets were resuspended in lysis buffer plus 500 mM (NH<sub>4</sub>)<sub>2</sub>SO<sub>4</sub>. NS3h was further purified using methyl-hydrophobic (30 ml), heparin-Sepharose (30 ml), and poly(U) affinity (20 ml) chromatography columns. NS3h was eluted from each column with a low salt/high salt buffer gradient (10 mM/1 M NaCl in 25

mM Tris/Cl, pH 7.5, 1 mM EDTA, 5 mM β-mercaptoethanol, 10% glycerol). The gradient was reversed for the hydrophobic column. NS3h eluted from the hydrophobic and heparin-Sepharose columns between 250 and 450 mM NaCl and from the poly(U) column between 450 and 650 mM NaCl. Fractions containing NS3h were combined and dialyzed into low salt buffer following elution from each column. Fractions from the final column were dialyzed into storage buffer (25 mM Tris/Cl, pH 7.5, 1 mM EDTA, 100 mM NaCl, 5 mM β-mercaptoethanol, 20% glycerol) and concentrated to 7–10 μM.

**Crystallization and Structural Determination of NS3h**—Purified NS3h was concentrated to 32.2 mg/ml for crystallization. Examination of sample purity and determination of molecular weight were performed using SDS-PAGE on a Phast Gel system (AP Biotech). The apparent molecular mass of the helicase was ~50 kDa. The (dU)<sub>16</sub> oligonucleotide was synthesized using an Expedite nucleic acid synthesis system and purified by polyacrylamide gel electrophoresis to a final concentration of 4.6 mg/ml. Immediately before crystallization, NS3h was mixed with the (dU)<sub>16</sub> oligonucleotide at a 2:1 molar ratio. Crystals of diffraction quality were obtained by using the hanging drop method at room temperature with 4 μl of the mixture and 1 μl of reservoir solution (2.4 M (NH<sub>4</sub>)<sub>2</sub>SO<sub>4</sub>, 0.1 M Tris hydrochloride, pH 8.5). Diffraction data were collected at 1.5418 Å by using a single crystal of 0.2 × 0.4 × 0.1 mm mounted in a thin-walled glass capillary at room temperature. The x-ray radiation was produced by an in-house Rigaku RU-H3RHB generator and focused by Osmic's Gutman multilayer mirrors (Woodland, TX). The diffraction pattern was recorded on the R-Axis IV phosphor image plate detector. The diffraction data were reduced, integrated, and scaled with Denzo/Scalepack. Molecular replacement analysis was performed using AMORE software (33), and structure refinements and model building/adjustment were done using CNS (34) and XtalView (35), respectively.

The scaled data of resolution 3.3 Å indicated that the NS3h/(dU)<sub>16</sub> crystal belongs to the orthorhombic space group (Table 1). Space group assignment between P2<sub>1</sub>2<sub>1</sub>2 and P2<sub>1</sub>2<sub>1</sub>2<sub>1</sub> could not be made due to the absence of some (00l) reflections. Matthews' coefficient suggested that the number of protein molecules in one asymmetric unit could be 3 or 4, with solvent content being 67 or 50%, respectively.

We completed the structure determination by molecular replacement (MR), using the published 1A1V structure (23) as an initial model. The 1A1V structure consists of an NS3h monomer bound to a (dU)<sub>8</sub> oligonucleotide. Prior to MR, the oligonucleotide was removed from the model. The MR results from space group P2<sub>1</sub>2<sub>1</sub>2 did not display any reasonable correlation among the individual solutions; however, the MR solutions in space group P2<sub>1</sub>2<sub>1</sub>2<sub>1</sub> showed strong correlation as well as realistic crystal packing (not shown).

A composite omit map was calculated using CNS (34) to identify any missing components. The resulting electron density map showed clearly the presence of the oligonucleotide at the nucleic acid binding sites of the protein molecules. The (dU)<sub>x</sub> fragments were inserted manually into the structure using XtalView (35). The maximum likelihood from structure factors refinement on the model was done in CNS and is presented in Table 1.

**Construction of Mutant Plasmids**—Mutations were introduced into a pUC18-NS3 subclone containing nucleotides 1182–4918 from the HCV-neo-I377/NS3–3'-untranslated region replicon sequence (GenBank™ accession number AJ242652) using the QuikChange site-directed mutagenesis kit (Stratagene). Mutant plasmids were transformed into SURE cells and purified from cultured cells with the QIAprep Spin Miniprep Kit (Qiagen). Mutant subcloned HCV sequences were then transferred into the replicon plasmid by digestion at PmeI and MluI

# Crystal Structure of Two NS3h Molecules Bound to the Same Strand of DNA

restriction sites followed by ligation. Mutant NS3 sequences were transferred to pET26b-ubiquitin expression plasmid by PCR followed by digestion at SacII and EcoRI restriction sites and ligation. Quality of all final plasmid products was confirmed by sequencing.

**Replicon RNA Synthesis**—DNA template was prepared by digestion of replicon plasmid (10  $\mu$ g) with ScaI restriction endonuclease at 37 °C for 4 h. Complete linearization of plasmid was confirmed by agarose gel electrophoresis. RNA was synthesized *in vitro* by incubating 0.5  $\mu$ g of linear DNA template with 0.5  $\mu$ g of T7 RNA polymerase in 350 mM HEPES, pH 7.5, 32 mM magnesium acetate, 40 mM dithiothreitol, 2 mM spermidine, and 28 mM NTPs at 37 °C for 3 h. Template DNA was removed by incubation with 2 units of DNase I at 37 °C for 30 min. RNA was precipitated overnight in LiCl at –20 °C. RNA purity and quality were verified by agarose gel electrophoresis.

**Colony Formation Assays**—Huh-7.5 cells were trypsinized 1 day before transfection. Cells ( $2 \times 10^6$ ) were washed once with DMEM lacking serum and suspended in 0.9 ml of the same medium. RNA-liposome complexes were prepared using the TransMessenger reagent from Qiagen. Cells and RNA-liposome complexes were mixed and incubated at 37 °C for 1 h. After incubation, cells were pelleted by centrifugation ( $525 \times g$ ) for 4 min and suspended in DMEM containing 10% fetal bovine serum. Cells were plated in 100-mm Petri dishes in the absence of feeder cells at the following densities:  $1 \times 10^6$ ,  $2 \times 10^5$ , and  $2 \times 10^4$ . After 2 days of recovery, cells were treated with 0.5 mg/ml G418, and selection was continued for 3 weeks with medium changes every 4 days. Cells were fixed and stained using crystal violet. At least three independent experiments were performed for each transfection.

**Western Analysis**—Huh-7.5 cells were transiently transfected with HCV RNA using TransMessenger Lipofectin Reagent (Qiagen) according to the manufacturer's instructions. Cells were lysed at 4 h post-transfection in SDS-PAGE denaturing sample buffer. Lysate from  $5 \times 10^5$  cells from each transfection was run on 10% SDS gel. Proteins were transferred from gel to polyvinylidene difluoride membrane using a Bio-Rad electrophoretic transfer cell at 100 V for 1 h at 4 °C in transfer buffer (25 mM Tris, 192 mM glycine). Membranes were blocked in 5% dry milk/TBST (20 mM Tris/Cl, pH 7.5, 137 mM NaCl, 0.1% Tween 20) for 1 h. Blocked membranes were exposed to rabbit polyclonal anti-NS3 in 5% bovine serum albumin/TBST for 90 min and then exposed to horseradish peroxidase-conjugated goat anti-rabbit IgG (PerkinElmer Life Sciences) in 5% dry milk/TBST for 1 h. Chemiluminescent detection was done by an ECL Western blotting analysis system (Amersham Biosciences).

**Nucleic Acid Binding Assays**—NS3h was incubated with 500 pM 5'-fluorescein labeled rU<sub>20</sub> (Integrated DNA Technologies) in 50 mM MOPS (pH 7.0), 10 mM NaCl, 50  $\mu$ M EDTA, 0.1 mg/ml bovine serum albumin for 5 min at 37 °C. Binding was measured as a function of fluorescence polarization using a Beacon fluorescence polarization instrument. Data were fit to a hyperbola using Kaleidagraph software.

**ATPase Assays**—NS3h was incubated with 5 mM ATP in 50 mM HEPES (pH 7.5), 0.5 mM EDTA, 10 mM MgCl<sub>2</sub>, 10 mM NaCl, 0.1 mg/ml bovine serum albumin, 4 mM phosphoenolpyruvate, 10 units/ml pyruvate kinase/lactate dehydrogenase, and 0.7 mg/ml NADH. Absorbance of NADH at 380 nm was measured at 1-s intervals for a period of 30 s in the presence of the indicated concentrations of poly(U). Hydrolysis rates were calculated using an extinction coefficient of  $1,210 \text{ M}^{-1} \text{ cm}^{-1}$  for NADH. Data were fit to a hyperbola using Kaleidagraph software.

**DNA Unwinding Assays**—Unwinding assays were carried out using a Quench-Flow apparatus (RQF-3, KinTek Instruments, Austin, TX) and a two-step mixing protocol (32). The temperature was held constant at 37 °C with a circulating water bath. Reactions were carried out in 25 mM

**TABLE 1**  
Data collection and refinement statistics

Parameter	Value
<b>Data collection</b>	
Unit cell	$\alpha = \beta = \gamma = 90^\circ$
A (Å)	108.3
B (Å)	109.8
C (Å)	183.4
Space group	P2 <sub>1</sub> 2 <sub>1</sub> 2 <sub>1</sub>
Wavelength (Å)	1.5418
Resolution (Å)	3.3
Unique reflections	33,594
Completeness (%)	91.1
$R_{\text{sym}}^a$ (%)	0.34
$\langle I/\sigma(I) \rangle$	4.4
<b>Refinement</b>	
Resolution (Å)	30 to 3.3
No. of reflections <sup>b</sup>	27,936 (1,673)
$R^{\text{bc}}$ (%)	24.8 (27.4)
Average B-factors (Å <sup>2</sup> )	34.25
r.m.s. deviation bond lengths (Å)	0.010
r.m.s. deviation bond angles (degrees)	1.495

<sup>a</sup>  $R_{\text{sym}} = \sum |I - \langle I \rangle| / \sum I$ , where  $I$  represents intensity.

<sup>b</sup> Value for  $R_{\text{free}}$  set containing 5% of randomly chosen reflections.

<sup>c</sup>  $r = \sum |F_o - F_c| / \sum F_o$ .

MOPS (pH 7.0), 10 mM NaCl, 0.1 mM EDTA, 2 mM  $\beta$ -mercaptoethanol, and 0.1 mg/ml bovine serum albumin; all concentrations are postmixing. NS3h (500 nM) was mixed with 2 nM DNA substrate (30-base pair duplex with 3' T15 overhang; the longer strand was radiolabeled with <sup>32</sup>P) for 10 s before adding 5 mM ATP, 10 mM MgCl<sub>2</sub>, 60 nM annealing trap (complementary to the displaced strand), and 100  $\mu$ M poly(dT) protein trap. The reaction was quenched after 0.1–15 s by ejection into a tube containing 200 mM EDTA, 0.7% SDS. Double- and single-stranded DNA were resolved on a native 20% polyacrylamide gel, detected using a PhosphorImager (Amersham Biosciences), and quantified using ImageQuant software. Bench top experiments were used to determine the amplitude of product formation under single turnover conditions. NS3h was added to substrate (2 nM), followed by a 10-s incubation. ATP (5 mM), MgCl<sub>2</sub> (10 mM), and a protein trap (poly(dT), 100  $\mu$ M) were added to initiate the unwinding reaction. The reaction was stopped after 10 s by adding 200 mM EDTA. Data were fit to Equation 1, using Kaleidagraph (Synergy Software, Reading, PA). This equation describes a five-step mechanism for DNA unwinding that is necessary to fit the substantial lag phase associated with unwinding of the substrate (32, 36, 37).

$$Y = A(1 - (1 + k_{\text{obs}} t + 1/2(k_{\text{obs}} t)^2 + 1/6(k_{\text{obs}} t)^3 + 1/24(k_{\text{obs}} t)^4)e^{-k_{\text{obs}} t}) \quad (\text{Eq. 1})$$

## RESULTS

**Crystallization and Structural Analysis of NS3h Bound to (dU)<sub>16</sub>**—Crystals of NS3h in the presence of (dU)<sub>16</sub> oligonucleotide belonged to space group P2<sub>1</sub>2<sub>1</sub>2<sub>1</sub> with unit cell dimensions  $a = 108.3 \text{ Å}$ ,  $b = 109.8 \text{ Å}$ , and  $c = 183.4 \text{ Å}$  (Table 1). We determined the structure by the MR method, using 1A1V.pdb (23) as an initial model, in which its (dU)<sub>8</sub> fragment was manually removed prior to the rotational function search. We identified three helicase molecules (chains A, B, and C in Fig. 1) per asymmetric unit in our structure, with two helicase molecules bound to a single (dU)<sub>16</sub> molecule. The final atomic model shows no major unfavorable steric interactions between the helicase molecules, and the crystal packing shows no conflicts between the protein molecules in adjacent asymmetric units. We found no apparent noncrystallographic symmetric operations among the three monomers in this helicase model, nor did we observe any dramatic differences among the monomers. All three helicase molecules retain the basic Y



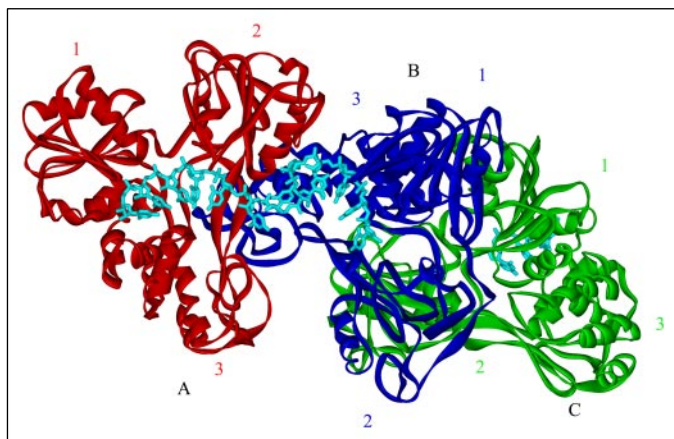


FIGURE 1. **X-ray crystal structure of NS3h bound to a 16-mer poly(dU) substrate.** Three molecules of NS3h are found in the asymmetric unit, and two of the helicase monomers, chain A (red) and chain B (blue), are bound to a single DNA substrate molecule (aqua). The third molecule of the asymmetric unit (chain C, shown in green) is bound to a separate strand of nucleic acid. The DNA passes across the face of chain A, emerging between domains 2 and 3, where it enters the binding site of chain B.

shape characteristic of previously reported structures, with minor conformational differences at the surface loop regions.

Chains A and B of the complex are bound to a 13-nucleotide span of one (dU)<sub>16</sub> molecule, with chain B rotated 90° relative to chain A. The binding mode of both chains is consistent with that of the 1A1V structure, with the binding cleft at the interface of domains 1 and 2 with domain 3 in each protein molecule. Chain C appears to be independent of the dimer-oligonucleotide complex. The nucleic acid binding cleft of chain C faces away from the dimer structure and is occupied by a second oligonucleotide molecule. Chain C does not have any evident structural or mechanistic relationship with the other two protein molecules, and there appear to be no suitable contacts between chains B and C to indicate a functional interaction between these two molecules.

To determine the degree of similarity between chains A and B, we superimposed the two using domain 1 (the NTPase domain) as an anchor (the backbone r.m.s. deviation for residues 190–324 was 0.7 Å). We observed only minor conformational differences between the two chains in each of the three domains (Fig. 2). However, it appears that the relative orientation of domain 2 with respect to the anchored domain 1 is slightly different between chains A and B with a small but detectable tilting angle, resulting in a slight widening of the nucleic acid binding groove in chain B. This flexibility of domain 2 relative to domain 1 is consistent with the ratchet mechanism for nucleic acid translocation proposed by Kim *et al.* (23). Domain 3 displays a small degree of rotation between chains A and B but is otherwise similar.

To assess the relationship of the apparent dimer structure to that of the monomeric NS3-oligonucleotide complex reported by Kim *et al.* (23), we independently aligned each of the two monomer structures (chains A and B) with the 1A1V structure (data not shown). Both chains of the dimer structure align well with 1A1V, with chain A being a slightly better fit than chain B (overall r.m.s. deviation ~0.9 and ~1.3 Å, respectively). Aside from the slight widening of the groove between domains 2 and 3 in chain B of our structure, no significant structural differences exist between the structure of 1A1V and the structures of our A and B chains.

In the dimer structure, the oligonucleotide is bound to each NS3h molecule within the groove formed at the interface of domains 1 and 2 with domain 3 (Fig. 1). The DNA interactions with chain A are virtually identical to those observed in the 1A1V structure. In the region between chains A and B, the DNA appears to be bent by nearly 90 degrees. It is

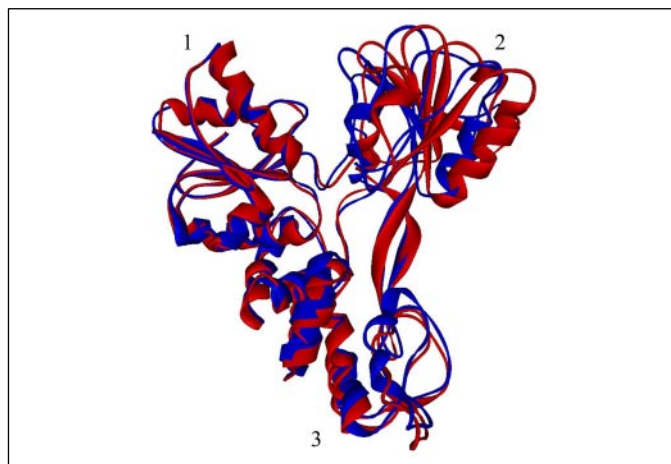


FIGURE 2. **Superposition of chains A (red) and B (blue) that comprise the NS3h dimer structure.** The two structures were superimposed using domain 1 (1) as an anchor and yielded an r.m.s. deviation of ~0.7 Å. Domain 2 of chain B (2) is tilted slightly relative to its position in chain A.

possible that this bend is stabilized by the apparent base stacking between nucleotides dU<sub>8</sub> and dU<sub>10</sub>. However, the electron density in this region is weak, and although structure validation by WHAT\_CHECK (38) suggested that the bent conformation of the DNA is allowable according to Parkinson (39), we accept the possibility that the bend may indeed exist in another conformation. Comparisons of the 3' binding regions in both chains A and B to 1A1V exhibited high similarity in nucleotide binding, suggesting that the binding mode of the oligonucleotide between chains A and B is likely to exist as presented. The overall DNA binding mode with respect to chain B is similar to that with respect to chain A (Fig. 3, A and B). However, due to the displacement of domain 2 in chain B, domains 2 and 3 are farther apart than in chain A. In turn, the binding groove of chain B is slightly wider and causes the oligonucleotide to tilt toward domain 2, allowing domain 1 and the oligonucleotide backbone to retain the same interactions observed in chain A. The domain displacement, however, does not dramatically alter the interactions of oligonucleotide with domains 1 and 3. For example, the Trp<sup>501</sup> side chain retains its ring-to-ring stacking position, and Thr<sup>269</sup> remains in position to allow hydrogen bonding with the phosphate backbone of the DNA at dU<sub>11</sub> (Fig. 3, A and B). The DNA fragment in chain B is pushed slightly out of the binding groove and shifted away from the  $\alpha$ -helical domain. As a result, the electron density for this fragment is less clear than that in chain A.

There are numerous close interactions between chains A and B involving multiple sets of amino acid residues, including His<sup>545</sup>–Ala<sup>553</sup> and Cys<sup>584</sup>–Thr<sup>591</sup> of chain B, and Thr<sup>435</sup>–Gln<sup>453</sup>, Thr<sup>477</sup>–Ser<sup>488</sup>, and Val<sup>524</sup>–Gln<sup>536</sup> of chain A (Fig. 4A). In addition, Thr<sup>450</sup> of chain A and Gln<sup>549</sup> of chain B appear to be in position to allow hydrogen bond formation between the two monomers at the dimeric interface (Fig. 4B). To assess the strength of interaction between chains A and B, we calculated the extent of buried surface area ( $S_{AB}$ ) at the interaction site using WHATIF molecular modeling software (40). This value is defined as  $S_{AB} = A_A + A_B - A_{AB}$ , where  $A$  is the total surface area of the folded polypeptide molecule. The surface areas of chains A and B are 5883 and 5839 Å<sup>2</sup>, respectively. The total surface area calculated for the dimer is ~11,279 Å<sup>2</sup>, leaving a difference of 443 Å<sup>2</sup> buried at the interface. This area is not sufficient to support independent dimer formation in the absence of nucleic acid, which is consistent with the observed monomeric behavior of NS3h in size exclusion chromatography.<sup>6</sup>

<sup>6</sup> K. D. Raney and Y. Chen, unpublished observations.

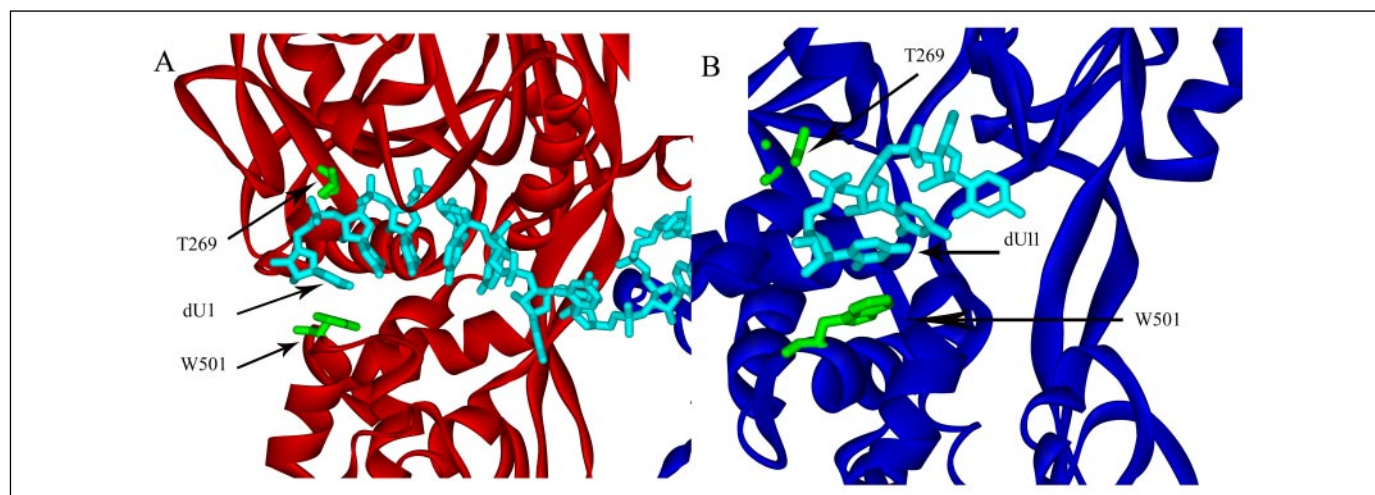


FIGURE 3. A, the terminal region of the oligonucleotide (aqua) interacts with NS3h chain A (red) via a hydrogen bond between Thr<sup>269</sup> (T269) and the phosphate backbone and ring stacking between nucleotide dU<sub>1</sub> and Trp<sup>501</sup> (W501; green). B, at the point where the oligonucleotide (aqua) enters the binding groove of chain B (blue), interactions identical to those with chain A are observed (Trp<sup>501</sup>-dU ring stacking and Thr<sup>269</sup>-phosphate hydrogen bond formation).

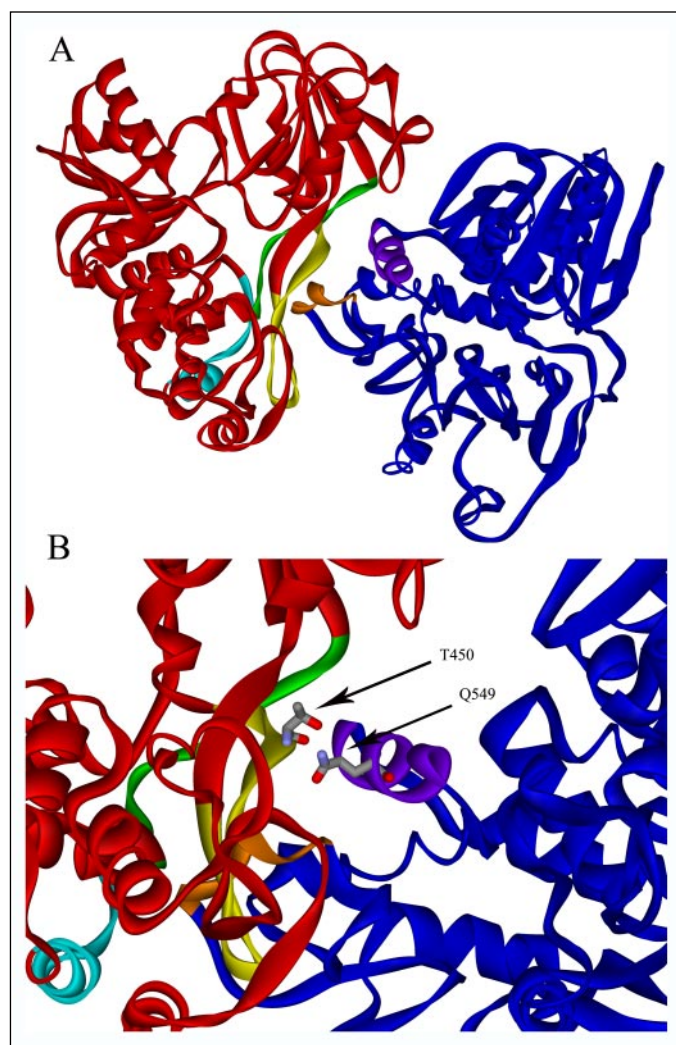


FIGURE 4. Depiction of the dimer structure involving chains A (red) and B (blue) illustrating the residues involved in the protein-protein interaction. A, five sets of residues are identified at the dimer interface, including His<sup>545</sup>-Ala<sup>553</sup> (purple) and Cys<sup>584</sup>-Thr<sup>591</sup> (orange) of chain B and Thr<sup>435</sup>-Gln<sup>453</sup> (yellow), Thr<sup>477</sup>-Ser<sup>488</sup> (green), and Val<sup>524</sup>-Gln<sup>536</sup> (cyan) of chain A. B, a close-up view of the dimer interface. A pair of hydrogen bonding partners, Thr<sup>450</sup> of chain A and Gln<sup>549</sup> of chain B, is highlighted.

**Biological Analysis of Surface Residues**—To assess the importance of the protein-protein interface region observed in the crystal structure, we performed a mutational analysis involving two clusters of residues (Asp<sup>543</sup>/His<sup>545</sup>/Gln<sup>549</sup> and Arg<sup>587</sup>/Leu<sup>588</sup>/Lys<sup>589</sup>/Thr<sup>591</sup>) in domain 3 (Fig. 4). These residues are situated at the interface of the two NS3h molecules and appear to be of particular importance in the protein-protein interaction. We did not introduce mutations at the domain 2 interface site because of its proximity to the conserved helicase motifs. Amino acid residues 543–545 were deleted ( $\Delta$ 543–545), and two sets of substitution mutations (D543K/H545D/Q549A and R587D/L588D/K589D/T591D) were introduced independently into the HCV-neo-I377/NS3–3′-untranslated region replicon (14) containing an S1179I adaptive mutation (12).

We transfected Huh-7.5 human hepatoma cells with mutant HCV RNA and monitored the cells for replication-dependent growth. Cells transfected with S1179I HCV RNA formed large, densely spaced colonies after 2–3 weeks of growth (Fig. 5A). Cells transfected with the mutant HCV RNA showed significantly reduced colony formation, indicating that the targeted NS3 surface region is important for efficient viral replication. The  $\Delta$ 543–545 and D543K/H545D/Q549A (NS3h KDA) mutants were of particular interest, since they supported little or no cell growth (Fig. 5, C and D). The R587D/L588D/K589D/T591D mutation (NS3h DDDD), at a different site within the protein interface than the  $\Delta$ 543–545 and NS3h KDA mutations, had a visible but less dramatic effect on growth (Fig. 5E).

We performed a Western analysis with NS3 antibody on transfected cell lysates in order to determine whether NS3 protein expression was affected by any of the mutations (Fig. 6). The  $\Delta$ 543–545 mutant NS3 protein was present at significantly lower concentration than observed in S1179I-transfected cells. However, no impairment of translation was observed for either of the two substitution mutants. Quantitative comparison with purified NS3h standards indicated that these similar expression levels were not an artifact of saturating assay conditions (supplemental Fig. 1).

**Biochemical Analysis of NS3h Mutants**—In order to determine the effects of the surface mutations on the biochemical activities of NS3h, we overexpressed and purified NS3h KDA and NS3h DDDD in a prokaryotic expression system and compared the binding and enzymatic activities of the mutant NS3h proteins with those of wild type. We measured the RNA binding affinity of the mutant and wild type enzymes



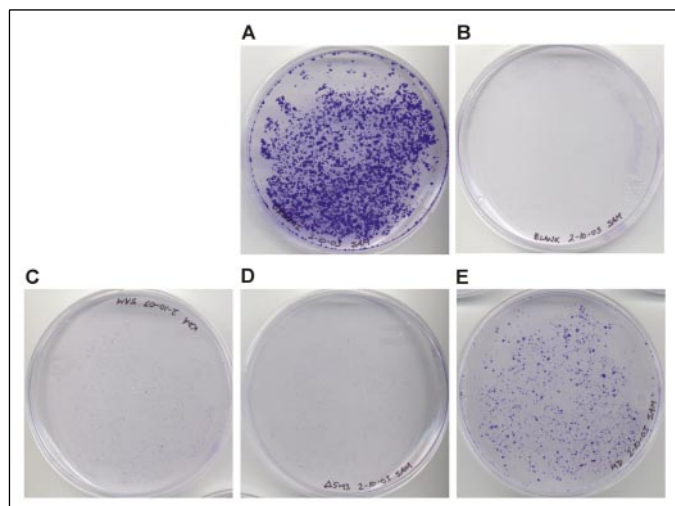


**FIGURE 5. Growth of Huh-7 cells after transfection with wild type and mutant forms of the HCV replicon.** Colony formation of Huh-7 cells was monitored over a period of 3 weeks following transfection by HCV replicon RNA. Colonies were stained with 0.1% crystal violet. Representative plate images for each transfection are as follows: A, S1179I RNA; B, blank transfection (no RNA); C, D543K/H545D/Q549A mutant RNA; D,  $\Delta$ 543–545 mutant RNA; E, R587D/L588D/K589D/T591D mutant RNA. Colony-forming units per microgram of RNA for each experiment were as follows:  $15,560 \pm 940$ ,  $2,720 \pm 440$ , and  $7,760 \pm 1,072$  for the S1179I RNA, D543K/H545D/Q549A mutant RNA, and R587D/L588D/K589D/T591D mutant RNA, respectively. No colonies were observed for the blank treatment or for the  $\Delta$ 543–545 mutant RNA.

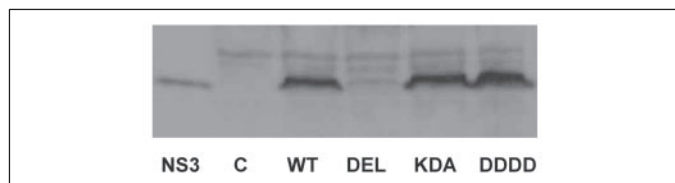


**FIGURE 6. Western analysis of HCV-transfected Huh-7.5 cell lysates.**  $5 \times 10^5$  cells from each lysate were loaded on a 10% polyacrylamide gel. The gel was blotted onto a polyvinylidene difluoride membrane, and the blot was incubated with rabbit anti-NS3. Primary antibody binding was detected by chemiluminescence with horseradish peroxidase-conjugated anti-rabbit IgG. The lane marked NS3 shows purified NS3. The lane marked C shows the control transfection with no HCV RNA. WT, wild type.

using a fluorescein-labeled oligonucleotide substrate (Fig. 7). The NS3h KDA mutation did not impair binding to RNA, but the NS3h DDDD mutation severely reduced binding affinity as measured by fluorescence polarization. Poly(U)-stimulated ATP hydrolysis of the mutant and wild type enzymes was measured, and no significant differences were observed between the activities of the wild type and NS3h KDA mutant (Fig. 8). The activity of the NS3h DDDD mutant was severely impaired, probably as a consequence of its reduced nucleic acid binding affinity.

Unwinding of nucleic acid was measured by using a standard helicase assay (Fig. 9A) with a substrate (45/30-mer) containing 30 base pairs with a 15-nucleotide 3' single-stranded overhang. Very little unwinding of an RNA substrate by NS3h was observed (Fig. 9B), consistent with a recent report describing the lack of RNA unwinding activity of NS3h (27), so unwinding rates were determined using a DNA substrate (30). Under single turnover conditions, NS3h exhibited a lag phase similar to that observed previously for a substrate of similar length (Fig. 10) (32). The lag phase represents multiple steps that are believed to occur prior to complete unwinding of the duplex (36, 37, 41). However, NS3h KDA unwound the substrate with a similar lag phase as the wild type enzyme but somewhat lower amplitude (Fig. 10). Very little unwinding was observed with NS3h DDDD, consistent with the poor binding to nucleic acid. The amplitude for unwinding reflects the degree of processivity of the enzyme (30, 32, 42); therefore, NS3h KDA has slightly lower proces-

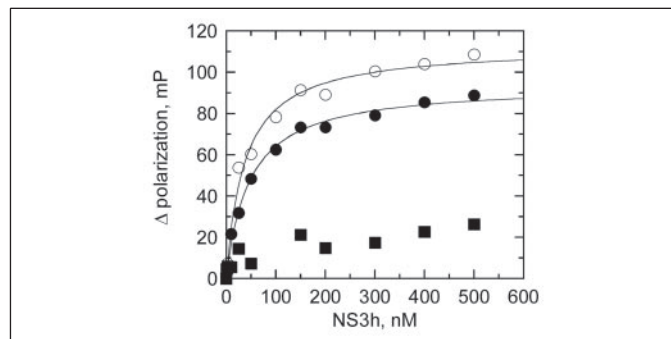


**FIGURE 7. Binding of mutant NS3h to fluorescein-labeled U<sub>20</sub> RNA.** Nucleic acid binding was determined by measuring fluorescence polarization following incubation of protein and nucleic acid at 37 °C. Data were fit to a hyperbola using Kaleidagraph software. A, NS3h wild type (●) bound to RNA with a  $K_D$  of  $47 \pm 5$  nM, and NS3h KDA (○) bound to RNA with a  $K_D$  of  $38 \pm 4$  nM. NS3h DDDD (■) did not bind with high enough affinity to determine a binding constant under these conditions.

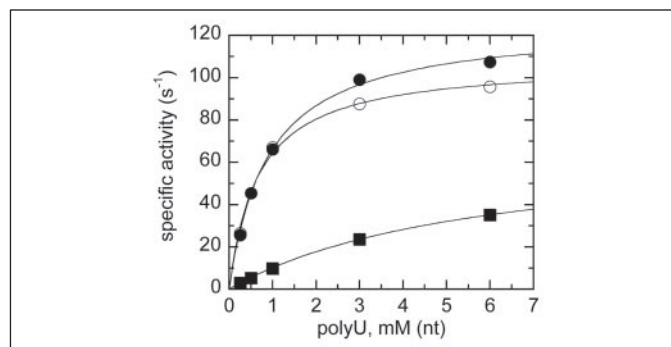


**FIGURE 8. ATPase activity of mutant NS3h (50 nM) was measured as a function of nucleic acid concentration in a coupled spectrophotometric assay.** Data represent the average of three independent experiments and were fit to a hyperbola using Kaleidagraph software. Specific activity of NS3h wild type (●) and NS3h KDA (○) were comparable at 126 and 108  $s^{-1}$ , respectively, in the presence of saturating poly(U). Specific activity of NS3h DDDD (■) was lower at 70  $s^{-1}$ . The concentration of nucleic acid ( $K_{act}$ ) required to reach one-half  $V_{max}$  was 0.89, 0.68, and 5.84  $\mu$ M for NS3h wild type, NS3h KDA, and NS3h DDDD, respectively.

sivity than NS3h. Increasing the enzyme concentration resulted in higher amplitudes for each enzyme. We previously reported that binding of multiple full-length NS3 molecules to this substrate increases the amplitude for unwinding (30). The results here with NS3h are consistent with the observation for full-length NS3.

## DISCUSSION

We describe here the first x-ray crystal structure of NS3 helicase bound to a DNA molecule of sufficient length to accommodate binding of two molecules of enzyme. Our structure shows a nucleic acid binding site for each monomer that is consistent with a published crystal structure of a single monomer bound to a shorter DNA molecule (23). In each case, the DNA binds to a cleft between domains 1 and 2 on one side and domain 3 on the other. DNA binding is not sequence-specific, with the majority of protein-DNA contacts involving the phosphate backbone. The structure also reveals a protein-protein interface between two DNA-bound helicase monomers. The protein-protein contacts are mostly hydrophobic and involve domain 2 of one subunit (chain A) and domain 3 of the second subunit (chain B). The two nucleic acid binding sites of the dimer are therefore aligned in such a way as to force a significant bend in the bound DNA that appears to induce a base stacking motif in the oligonucleotide.

The structure and function of HCV helicase have been investigated extensively. Important amino acid sequence motifs that play critical roles in biochemical function have been identified in both domains 1

## Crystal Structure of Two NS3h Molecules Bound to the Same Strand of DNA

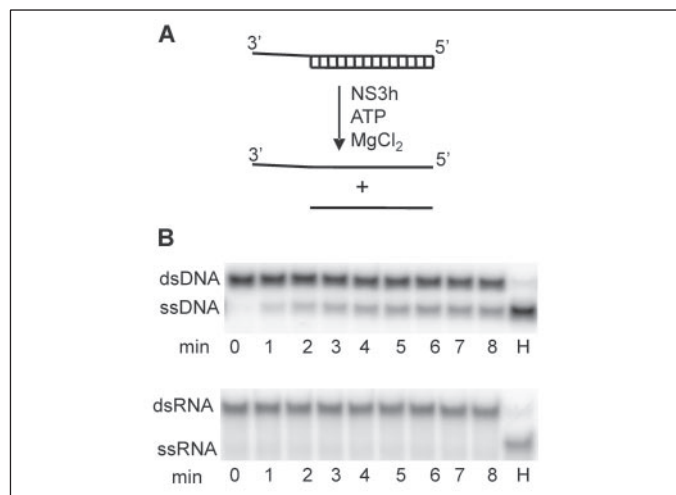


FIGURE 9. **A**, the assay for measuring helicase unwinding activity is depicted. A partial duplex substrate containing 30 bp and 15 nucleotides of single-stranded overhang (45/30-mer) was incubated with NS3h in the presence of ATP and  $Mg^{2+}$ , leading to unwinding of the duplex. **B**, comparison of unwinding of DNA and RNA substrates by NS3h (representative gels). Otherwise identical 250 nM duplexed DNA and RNA substrates were incubated with 100 nM NS3h. Reactions were initiated by the addition of 5 mM ATP and 10 mM  $MgCl_2$  and quenched by the addition of 200 mM EDTA, 0.7% SDS. ssDNA and ssRNA, single-stranded DNA and RNA, respectively; dsDNA and dsRNA, double-stranded DNA and RNA, respectively.

and 2. The function of domain 3 has been less well characterized. Domain 3 of superfamily II helicases is less conserved compared with domains 1 and 2, and there is no apparent homology in domain 3 among the different helicase superfamilies (43). However, the sequence of domain 3 is highly conserved among HCV isolates (supplemental Fig. 2). In the structure reported here, surface regions on domain 3 appear to interact with domain 2 of the second molecule. Biological studies demonstrate that mutations in these surface regions interfere with viral replication in cell culture. Although it remains difficult to speculate as to its precise function, domain 3 may play a role in mediating the formation of protein-protein complexes between NS3 monomers or between NS3 and other proteins in addition to its critical role in substrate binding.

Several models for helicase function of NS3 have been proposed. Each mechanism is driven by binding and hydrolysis of ATP, which is thought to drive the enzyme through multiple conformational states. One model is the proposed inchworm-type mechanism in which the helicase repeatedly releases and rebinds a single strand of the nucleic acid substrate. Such a mechanism has been described for PcrA helicase (44) as well as for NS3h (45). The structure reported here shows two interacting monomers bound in series to the same DNA strand. Helicases that dimerize have been studied extensively by the Lohman laboratory, and a dimeric inchworm model has been suggested for *E. coli* Rep helicase (46). The alignment of the NS3h molecules along nucleic acid would favor some form of inchworm mechanism rather than a hand-over-hand mechanism, because the protein interface does not appear to be sufficient to maintain protein-protein interactions in the absence of nucleic acid binding. It is interesting that the dimeric structure reported here does not appear to impede flexible motions between domains 1 and 2 of the enzyme that are proposed to play a role in the inchworm mechanism (23). A model for NS3h activity involving Brownian motion was recently proposed based on the observation of two states of DNA binding (strong affinity and weak affinity) in the presence or absence of ATP (47). This "Brownian motor" model does not require protein-protein interactions for helicase activity. However, the model suggests that when multiple NS3h molecules bind to the same substrate molecule, the adjacent enzymes may enhance the net

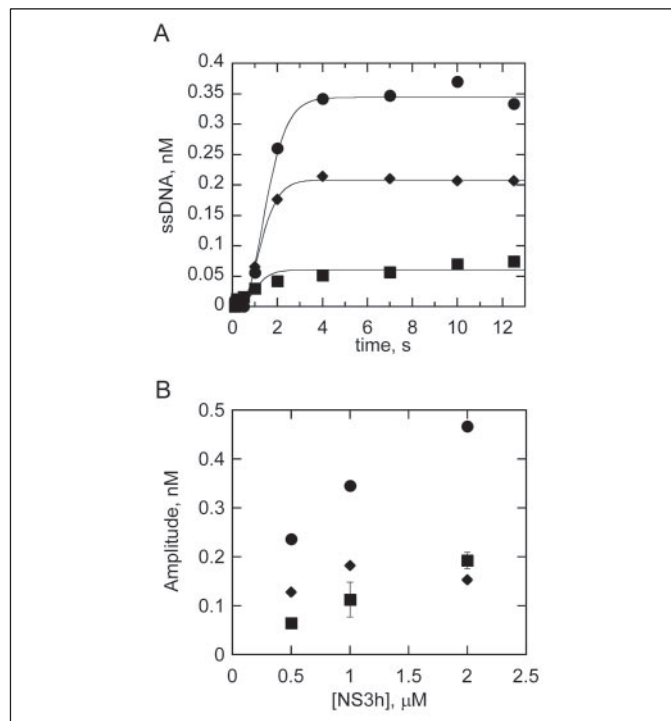


FIGURE 10. **A two-step mixing technique was used to measure single-turnover unwinding in the presence of excess NS3h.** **A**, NS3h (1  $\mu$ M) or one of the mutant enzymes was rapidly mixed with substrate followed by a 10-s incubation. A second, rapid mixing step followed, in which ATP,  $Mg^{2+}$ , and protein trap (poly(dT)) were added. The quench solution was placed in the receiving vial. Single-stranded DNA (ssDNA) was separated from double-stranded DNA by native polyacrylamide electrophoresis, and the fractions were quantified by using ImageQuant software. Data were fit according to Equation 1, resulting in unwinding rates of  $3.1 \pm 0.1$  s $^{-1}$ ,  $3.7 \pm 0.1$  s $^{-1}$ , and  $4.5 \pm 0.9$  s $^{-1}$  for NS3h (●), NS3h KDA (◆), and NS3h DDDD (■), respectively. **B**, unwinding amplitude versus concentration of NS3h and NS3h mutant enzymes. Bench top experiments were used to determine the amplitude of product formation under single turnover conditions. The amplitudes for NS3h (●), NS3h KDA (◆), and NS3h DDDD (■) were plotted as a function of enzyme concentration. The error bars represent S.D. of triplicate measurements.

activity by reducing the possibility for backwards sliding of the helicase during the unwinding cycle. Our own work is consistent with this general concept, in which multiple molecules of helicase bound to the same substrate enhance unwinding activity (30).

Recently, a model for unwinding by full-length NS3 was proposed that suggests a dimeric form of the enzyme based in part on an 18-bp step size determined by high resolution kinetic measurements (25). The structure reported here is consistent with the proposed dimeric form of the enzyme. However, unwinding data for the full-length form of NS3 indicate that a larger oligomer or substrate saturation may be required for optimal activity (30). NS3 is reportedly less processive in the absence of its co-factor, NS4A (42), so final conclusions regarding the oligomeric form required for optimal unwinding await detailed kinetic and biophysical studies of the NS3-4A complex. NS3h exhibits relatively weak protein-protein interactions, whereas full-length NS3 appears to interact with itself more strongly,<sup>7</sup> which may account for some of the differences in activities observed between the two forms of the enzyme. For example, NS3h unwound only 17% of the 45/30-mer (Fig. 10), whereas full-length NS3 unwound greater than 80% of the same substrate under the same conditions (30). Therefore, NS3h exhibits lower processivity in DNA unwinding than the full-length protein, which may reflect the relative strength of protein-protein interactions.

The mutations at the interface of the putative NS3h dimer were

<sup>7</sup> K. D. Raney and Y. Chen, manuscript in preparation.

designed to disrupt protein-protein interactions. These mutations would not be expected to disrupt the biochemical activities of monomeric NS3h. Indeed, NS3h KDA exhibits activities that mirror the wild-type enzyme in terms of nucleic acid binding and ATPase activity. The only biochemical activity of NS3h KDA that is reduced is processivity, which may reflect reduced protein-protein interactions. However, the reduction in amplitude for unwinding under single turnover conditions is only ~2-fold, which would seem unlikely to be responsible for the dramatic reduction in HCV replicative capacity exhibited with the NS3h KDA mutations. Hence, the biochemical results are not sufficient to explain the biological results. The results with NS3h DDDD further emphasize this point. NS3h DDDD has much lower affinity for nucleic acid than wild-type NS3h, resulting in little product formation under single turnover unwinding conditions. However, the replicative capacity of the HCV replicon containing the DDDD mutation is greater than the HCV replicon containing the KDA mutation. Thus, the biochemical activities that are typically measured of NS3h do not appear to reflect all of the biological activities of this enzyme.

It remains a strong possibility that the protein surface implicated in formation of a dimeric helicase *in vitro* mediates additional interactions *in vivo* that are required for formation of a multiprotein viral replication complex. For example, this protein surface might bind to the NS5B RNA polymerase to form part of the HCV replication machinery. NS5B has been shown to interact with NS3 (48). Several reports support the idea that HCV replication takes place at specific membrane-associated sites (17, 49, 50). NS3, NS5B, and other nonstructural viral proteins co-localize in replicon-transfected cells within the endoplasmic reticulum (17). A recent report suggests that lipid rafts may support viral replication (18). Insertion of active viral transcription complexes into cellular membranes would presumably require some sort of coordinated membrane-targeting and assembly process. It is reasonable to hypothesize that this assembly process requires specific protein-protein and protein-DNA interactions that are not necessary for *in vitro* enzyme activity. The crystal structure described here may represent a protein complex required for some function of NS3 not directly related to unwinding. For example, the helicase dimer (or larger oligomer) may sequester single-stranded nucleic acids that have already been acted on by the HCV replication machinery or may play a role in formation of viral RNA secondary structures required for initiation of transcription or translation. A recent report suggests that HCV RNA is an integral part of a viral nucleoprotein replication complex (18). The protein-protein interaction suggested by the crystal structure could be a subunit of such a complex.

By solving the x-ray crystal structure of two molecules of NS3 helicase bound to the same oligonucleotide, we have identified a region on the surface of the protein that is required for efficient viral replication. The amino acid residues in this region are highly conserved among different HCV isolates. The surface region appears to be capable of mediating protein-protein interactions but does not appear to be essential in the nucleic acid binding or known enzymatic activities of NS3h. These data illustrate that NS3 has additional biochemical activities and/or mediates protein-protein interactions *in vivo* through domain 3 that are not reflected in standard helicase assays.

**Acknowledgments**—We thank Brandy Tharp and Jamie Arnold for providing technical assistance and Robert Eoff for synthesis and purification of oligonucleotides.

## REFERENCES

1. Tan, S. L., Pause, A., Shi, Y., and Sonenberg, N. (2002) *Nat. Rev. Drug Discov.* **1**, 867–881
2. Giannini, C., and Brechot, C. (2003) *Cell Death. Differ.* **10**, Suppl. 1, S27–S38
3. Penin, F., Dubuisson, J., Rey, F. A., Moradpour, D., and Pawlowsky, J. M. (2004) *Hepa-*

- tology* **39**, 5–19
4. De Francesco, R., and Rice, C. M. (2003) *Clin. Liver Dis.* **7**, 211–242
5. Blight, K. J., Kolykhalov, A. A., Reed, K. E., Agapov, E. V., and Rice, C. M. (1998) *Antivir. Ther.* **3**, 71–81
6. Reed, K. E., Grakoui, A., and Rice, C. M. (1995) *J. Virol.* **69**, 4127–4136
7. Bartenschlager, R., Ahlborn-Laake, L., Mous, J., and Jacobsen, H. (1993) *J. Virol.* **67**, 3835–3844
8. Kim, D. W., Gwack, Y., Han, J. H., and Choe, J. (1995) *Biochem. Biophys. Res. Commun.* **215**, 160–166
9. Failla, C., Tomei, L., and De Francesco, R. (1994) *J. Virol.* **68**, 3753–3760
10. Behrens, S. E., Tomei, L., and De Francesco, R. (1996) *EMBO J.* **15**, 12–22
11. Enomoto, N., Sakuma, I., Asahina, Y., Kurosaki, M., Murakami, T., Yamamoto, C., Izumi, N., Marumo, F., and Sato, C. (1995) *J. Clin. Invest.* **96**, 224–230
12. Blight, K. J., Kolykhalov, A. A., and Rice, C. M. (2000) *Science* **290**, 1972–1974
13. Heller, T., Saito, S., Auerbach, J., Williams, T., Moreen, T. R., Jazwinski, A., Cruz, B., Jeurkar, N., Sapp, R., Luo, G., and Liang, T. J. (2005) *Proc. Natl. Acad. Sci. U. S. A.*
14. Lohmann, V., Korner, F., Koch, J., Herian, U., Theilmann, L., and Bartenschlager, R. (1999) *Science* **285**, 110–113
15. Lin, C., Thomson, J. A., and Rice, C. M. (1995) *J. Virol.* **69**, 4373–4380
16. Qin, W., Luo, H., Nomura, T., Hayashi, N., Yamashita, T., and Murakami, S. (2002) *J. Biol. Chem.* **277**, 2132–2137
17. Mottola, G., Cardinali, G., Ceccacci, A., Trozzi, C., Bartholomew, L., Torrisi, M. R., Pedrazzini, E., Bonatti, S., and Migliaccio, G. (2002) *Virology* **293**, 31–43
18. Shi, S. T., Lee, K. J., Aizaki, H., Hwang, S. B., and Lai, M. M. (2003) *J. Virol.* **77**, 4160–4168
19. Delagoutte, E., and von Hippel, P. H. (2002) *Q. Rev. Biophys.* **35**, 431–478
20. Delagoutte, E., and von Hippel, P. H. (2003) *Q. Rev. Biophys.* **36**, 1–69
21. Hall, M. C., and Matson, S. W. (1999) *Mol. Microbiol.* **35**, 867–877
22. Cho, H. S., Ha, N. C., Kang, L. W., Chung, K. M., Back, S. H., Jang, S. K., and Oh, B. H. (1998) *J. Biol. Chem.* **273**, 15045–15052
23. Kim, J. L., Morgenstern, K. A., Griffith, J. P., Dwyer, M. D., Thomson, J. A., Murcko, M. A., Lin, C., and Caron, P. R. (1998) *Structure* **6**, 89–100
24. Gallinari, P., Brennan, D., Nardi, C., Brunetti, M., Tomei, L., Steinkuhler, C., and De Francesco, R. (1998) *J. Virol.* **72**, 6758–6769
25. Serebrov, V., and Pyle, A. M. (2004) *Nature* **430**, 476–480
26. Locatelli, G. A., Spadari, S., and Maga, G. (2002) *Biochemistry* **41**, 10332–10342
27. Frick, D. N., Rypma, R. S., Lam, A. M., and Gu, B. (2004) *J. Biol. Chem.* **279**, 1269–1280
28. Levin, M. K., and Patel, S. S. (1999) *J. Biol. Chem.* **274**, 31839–31846
29. Yao, N., Reichert, P., Taremi, S. S., Prosser, W. W., and Weber, P. C. (1999) *Struct. Fold Des* **7**, 1353–1363
30. Tackett, A. J., Chen, Y., Cameron, C. E., and Raney, K. D. (2005) *J. Biol. Chem.* **280**, 10797–10806
31. Levin, M. K., and Patel, S. S. (2002) *J. Biol. Chem.* **277**, 29377–29385
32. Levin, M. K., Wang, Y. H., and Patel, S. S. (2004) *J. Biol. Chem.* **279**, 26005–26012
33. Navaza, J. (2001) *Acta Crystallogr. D Biol. Crystallogr.* **57**, 1367–1372
34. Brunger, A. T., Adams, P. D., Clore, G. M., DeLano, W. L., Gros, P., Grosse-Kunstleve, R. W., Jiang, J. S., Kuszewski, J., Nilges, M., Pannu, N. S., Read, R. J., Rice, L. M., Simonson, T., and Warren, G. L. (1998) *Acta Crystallogr. D Biol. Crystallogr.* **54**, 905–921
35. McRee, D. E. (1999) *J. Struct. Biol.* **125**, 156–165
36. Ali, J. A., and Lohman, T. M. (1997) *Science* **275**, 377–380
37. Lucius, A. L., Maluf, N. K., Fischer, C. J., and Lohman, T. M. (2003) *Biophys. J.* **85**, 2224–2239
38. Hooft, R. W., Vriend, G., Sander, C., and Abola, E. E. (1996) *Nature* **381**, 272
39. Parkinson, G. (1996) *Acta Crystallogr. Sect. D* **52**, 57–64
40. Vriend, G. (1990) *J. Mol. Graph.* **8**, 52–56
41. Galletto, R., Jezewska, M. J., and Bujalowski, W. (2004) *J. Mol. Biol.* **343**, 83–99
42. Pang, P. S., Jankowsky, E., Planet, P. J., and Pyle, A. M. (2002) *EMBO J.* **21**, 1168–1176
43. Singleton, M. R., and Wigley, D. B. (2002) *J. Bacteriol.* **184**, 1819–1826
44. Velankar, S. S., Soutanas, P., Dillingham, M. S., Subramanya, H. S., and Wigley, D. B. (1999) *Cell* **97**, 75–84
45. Kim, J. L., Morgenstern, K. A., Lin, C., Fox, T., Dwyer, M. D., Landro, J. A., Chambers, S. P., Markland, W., Lepre, C. A., O'Malley, E. T., Harbeson, S. L., Rice, C. M., Murcko, M. A., Caron, P. R., and Thomson, J. A. (1996) *Cell* **87**, 343–355
46. Cheng, W., Brendza, K. M., Gauss, G. H., Korolev, S., Waksman, G., and Lohman, T. M. (2002) *Proc. Natl. Acad. Sci. U. S. A.* **99**, 16006–16011
47. Levin, M. K., Gurjar, M. M., and Patel, S. S. (2003) *J. Biol. Chem.* **278**, 23311–23316
48. Piccininni, S., Varaklioti, A., Nardelli, M., Dave, B., Raney, K. D., and McCarthy, J. E. (2002) *J. Biol. Chem.* **277**, 45670–45679
49. Wolk, B., Sansonno, D., Krausslich, H. G., Dammacco, F., Rice, C. M., Blum, H. E., and Moradpour, D. (2000) *J. Virol.* **74**, 2293–2304
50. Hugle, T., Fehrmann, F., Bieck, E., Kohara, M., Krausslich, H. G., Rice, C. M., Blum, H. E., and Moradpour, D. (2001) *Virology* **284**, 70–81



**Structural and Biological Identification of Residues on the Surface of NS3 Helicase  
Required for Optimal Replication of the Hepatitis C Virus**

Samuel G. Mackintosh, Jeff Zhiqiang Lu, John B. Jordan, Melody K. Harrison, Bartek Sikora, Suresh D. Sharma, Craig E. Cameron, Kevin D. Raney and Joshua Sakon

*J. Biol. Chem.* 2006, 281:3528-3535.

doi: 10.1074/jbc.M512100200 originally published online November 22, 2005

---

Access the most updated version of this article at doi: [10.1074/jbc.M512100200](https://doi.org/10.1074/jbc.M512100200)

Alerts:

- [When this article is cited](#)
- [When a correction for this article is posted](#)

[Click here](#) to choose from all of JBC's e-mail alerts

Supplemental material:

<http://www.jbc.org/content/suppl/2005/11/23/M512100200.DC1>

This article cites 49 references, 22 of which can be accessed free at  
<http://www.jbc.org/content/281/6/3528.full.html#ref-list-1>